Geology

Direct calibration of salt sheet kinematics during gravity-driven deformation

--Manuscript Draft--

Manuscript Number:	G40219R1
Full Title:	Direct calibration of salt sheet kinematics during gravity-driven deformation
Short Title:	The internal kinematics of a thick salt sheet
Article Type:	Article
Keywords:	Salt; Fluid escape pipes; Salt viscosity; salt flow
Corresponding Author:	Joe Cartwright oxford university UNITED KINGDOM
Corresponding Author Secondary Information:	
Corresponding Author's Institution:	oxford university
Corresponding Author's Secondary Institution:	
First Author:	Joe Cartwright
First Author Secondary Information:	
Order of Authors:	Joe Cartwright
	Chris Kirkham
	Neil Hodgson
	Karyna Rodriguez
Order of Authors Secondary Information:	
Manuscript Region of Origin:	LEBANON
Abstract:	Three-dimensional (3-D) seismic imaging techniques are used to identify a series of 21 deformed fluid escape pipes that transected a 1500 m thick salt sheet at regular intervals over the past 1.7 myrs. By reconstructing these pipes to their original vertical cylindrical geometry, we show that the salt sheet deformed by Couette Flow over this period. The average flow velocity of the top boundary of 2 (+/- 0.3) mm/a, equates to a bulk viscosity for the sheet of 2.3.1018 Pa s, within the range obtained from field and laboratory measurements. Similar fluid escape structures are expected to occur widely in salt basins due to the extreme fluid overpressure developed beneath the almost impermeable salt. These structures offer a new approach for constraining basin-scale models of the kinematics of salt flow by the in situ measurement of flow geometry, with the potential to provide calibrations for experimentally derived flow laws for evaporite systems.

Publisher: GSA
Journal: GEOL: Geology
DOI:10.1130/G40219.1

Direct calibration of salt sheet kinematics during gravity-driven deformation

Joe Cartwright[1], Chris Kirkham[1], Claudia Bertoni[1], Neil Hodgson[2], and Karyna Rodriguez[2]

[1]*Department of Earth Sciences, University of Oxford, Oxford, OX1 3 AN, UK*

[2]*SpectrumGeo Ltd. Dukes Court, Woking, Surrey, GU21 5BH, UK*

ABSTRACT

Three-dimensional (3-D) seismic imaging techniques are used to identify a series of 21 deformed fluid escape pipes that transected a 1500 m thick salt sheet at regular intervals over the past 1.7 myrs. By reconstructing these pipes to their original vertical cylindrical geometry, we show that the salt sheet deformed by Couette Flow over this period. The average flow velocity of the top boundary of 2 (+/– 0.3) mm/a, equates to a bulk viscosity for the sheet of $2.3.10^{18}$ Pa s, within the range obtained from field and laboratory measurements. Similar fluid escape structures are expected to occur widely in salt basins due to the extreme fluid overpressure developed beneath the almost impermeable salt. These structures offer a new approach for constraining basin-scale models of the kinematics of salt flow by the in situ measurement of flow geometry, with the potential to provide calibrations for experimentally derived flow laws for evaporite systems.

INTRODUCTION

Kilometres thick, autochthonous salt sheets are widely developed in the geological record, and their gravity-driven deformation has had a major influence on

controlling the structure and stratigraphy of many passive continental margin, rift and foreland basins, from the Proterozoic to the Recent (Jackson and Hudec, 2017). Testing the contrasting modes of salt sheet flow regime (e.g., Poiseulle versus Couette) and relating them to the driving and boundary conditions is a major goal of salt tectonics (Brun and Fort, 2011) and has major practical implications for safe drilling through salt (Weijermaars and Jackson, 2014). Accurate modeling of salt sheet behavior therefore clearly requires realistic input of the salt rheology (Gemmer et al., 2004).

To date, no direct in situ measurements of viscosity from basin-scale deforming salt sheets have been made over an appropriate time scale (i.e., millions of years) that would characterise the effective rheology of the natural salt system, although attempts have been made to invert for the rheology using numerical modelling (Li et al., 2012). Direct measurements of salt flow velocity have thus far only been made on human observation time scales using surface measurements, and only then on extrusive salt bodies and salt diapirs rather than autochthonous salt sheets (Jackson and Hudec, 2017).

Here, we present the first direct calibration of the internal flow velocity of a thick (>1.5 km) salt sheet deforming under gravity. This allows us to compute the shear strain rate and the dynamic viscosity for a 2 Myr long period of continuous flow. This measurement resulted from the identification and three-dimensional mapping of a series of 21 fluid escape pipes, intruded through the salt sheet episodically during its deformation. We propose that fluid escape pipes represent a new class of geological strain marker, and suggest that they may be widely developed in other basins with thick evaporite layers. This new class of strain marker has the potential to provide constraints

on salt sheet deformation that should help refine existing numerical models of salt tectonics more generally.

Geological Setting

The study area is in the Levant Basin, where a c. 1.5 km thick Messinian evaporite sequence deposited during the Messinian Salinity Crisis (MSC) floors much of the deeper part of the basin (Gradmann et al., 2005)(Fig. 1). Marginal uplift and differential loading has led to widespread salt flow, with lateral extension around the basin margins and lateral contractional salt tectonics in the basin center (Cartwright and Jackson, 2008) (Fig. 1B). Bulk strain is relatively low (< 10%) in both the extensional and contractional domains with limited diapirism or dissolution of the salt (Fig. 1D). The internal structure of the deformed salt is well imaged by a set of laterally correlatable seismic reflections generated by thin clastic inter-layers (Feng et al., 2016)(Figs. 1C and D).

Gravity tectonics detaching in the thick salt sheet commenced in some areas during the latest Messinian (Bertoni and Cartwright, 2007; Gvirtzman et al., 2013; Feng et al., 2016), followed by a second phase in the Late Pliocene (Cartwright et al., 2012). The gross kinematics of WNW directed, basinward flow of the salt during this latest phase of deformation was orthogonal to the strike of the extensional faults and minor folds developed within the clay-dominated post-Messinian sequence (Fig. 1B and 1D). This regional flow regime for the eastern margin of the Levant Basin is consistent with gravity tectonics driven by basinward tilting of the margin combined with an element of differential loading between the slope and basin floor (Cartwright and Jackson, 2008; Gvirtzman et al., 2013). Rapid loading and unloading during and immediately after the

MSC led to widespread focused fluid escape from highly overpressured pre-salt sequences (Bertoni et al., 2017). This fluid escape resulted in numerous mapped examples of dissolution collapse structures, mud volcanoes and fluid escape pipes, identified throughout the Eastern Mediterranean using two-dimensional (2-D) and three-dimensional (3-D) seismic data (Reiche et al., 2014; Kirkham et al., 2017).

3-D Seismic Imaging of Fluid Escape Structures

Seismic Database and Interpretation Methodology

The three dimensional multichannel reflection seismic data used in the study were acquired by Spectrum in 2014, and covers an area of 5350 km^2 of the Lebanese continental slope between water depths of 1750 and 2050 m. Seismic interpretation was performed using Schlumberger's Petrel 3-D seismic software platform. Horizons were picked manually and auto-correlated and used to generate root mean square (RMS) amplitude maps. Coherence and RMS amplitude volumes were computed and interpreted in time slice form to identify key structural and fluid-related features based on recognized interpretational analogues (Cartwright and Santamarina, 2015; Kirkham et al., 2017)(see Data Repository).

3-D Seismic Interpretation

We identified a previously unknown major locus for deep-seated fluid escape close to the center of the high resolution 3-D reflection seismic volume (Figs. 1B and 2A). The locus of this fluid escape is indicated by a 500 m diameter pockmark crater of probable Holocene age mapped on the modern seabed (Fig. 2B, Fig. DR1). The pockmark is the upper terminus of a vertical, cylindrical fluid escape pipe, directly comparable to those seen in many other basins and generally interpreted to form by

hydraulic fracturing (Cartwright and Santamarina, 2015). Similar fluid escape pipes have recently been identified crossing thick Messinian salt sheets offshore Egypt, where they act as feeders for small mud volcanoes. These have also been attributed to hydraulic fracturing (Kirkham et al. 2017), although dilatancy in the salt under high pressure may contribute to the permeability of the pipe structure (c.f. Kukla et al. 2011). This c. 150 m wide, and > 2000 m tall pipe is interpreted to root in Early Miocene sandstone reservoirs at the crest of a prominent NNE-SSW trending pre-salt anticline (Fold A)(Figs. 2A and 2B; Figs. DR1 and DR2). The pipe is interpreted from abrupt stratal reflection terminations (see Data Repository) crossing mid-late Miocene claystones, Messinian evaporites and Pliocene to Recent claystones. Acoustically soft amplitude 'soft' anomalies adjacent to the pipe (Fig. 2D; Fig. DR2) are indicative of shallow gas accumulations (Judd and Hovland, 2009). This is consistent with the pipe acting as a conduit for gas during pipe formation, as is commonly observed in many other fluid escape pipes and mud volcano conduits (Kirkham et al., 2017).

Volumetric interpretation of the coherence attribute volume (see Data Repository) resulted in the identification of an additional 20 pockmarks of similar dimensions to the modern pockmark (Fig. 2; Figs. DR2 and DR3). The 21 pockmarks are strongly aligned (Fig. 2A; Fig. DR3), individually incising into successively younging seismic horizons in a ESE direction (Fig. 2B, C and D). Each pockmark is underlain by a vertical zone of stratal disruption that extends downwards within the post-salt overburden succession to terminate within a zone of highly disrupted reflections within the Messinian Evaporites (Figs. 2C and 2D).

Publisher: GSA
Journal: GEOL: Geology
DOI:10.1130/G40219.1

Trails of amplitude anomalies observed in horizontal slices within the evaporite units in the root mean square (RMS) amplitude volume match the trail seen in horizontal slices through the coherence attribute volume (Fig. DR3). The disrupted intra-Messinian seismic reflections beneath the linearly aligned pockmark trail are bounded by a single, continuous, gently curved reflection (Reflection X) that dips at an average of 16° from a position directly beneath the oldest pockmark to the crest of the anticline at the Base Salt horizon (Fig. 2B; Fig. DR1). This inclined reflection is narrow, measuring c. 150 m across on profiles extracted from the volume on trajectories orthogonal to the pockmark trail. The narrow width of this inclined Reflection X means that it cannot be interpreted as one of the many intra-Messinian shear zones that are widely developed in the Levant Basin (Fig. 2B; Fig. DR2). These typically extend for many kilometres along their strike (Cartwright et al., 2012; Gvirtzman et al., 2013). Seismic profiles from either side of the pockmark trail show a remarkably consistent intra-Messinian deformational geometry (Fig. DR2). This implies that the seismic character of both Reflection X and the immediately overlying evaporites represent an acoustic fabric that was superimposed on the already deformed evaporites within the narrow corridor delimited by the pockmark trail.

DISCUSSION

We interpret Reflection X as a deformed fluid expulsion pipe that was originally vertical when it was emplaced at the time of formation of the first pockmark. We date the formation of this fluid expulsion pipe as 1.7 Ma (+/– 0.3 Ma) by tracing the horizon hosting the pockmark fed by this pipe to stratigraphically calibrated exploration

Publisher: GSA
Journal: GEOL: Geology
DOI:10.1130/G40219.1

boreholes (see Data Repository). Subsequent flow of the Messinian Evaporites led to shearing of the pipe (Fig. 3).

By interpolation between the oldest and youngest pockmark, all intervening pockmarks would also be linked to their own individual feeder pipes. Their trajectories through the salt would also have been vertical at the time of formation, emanating from a common point in the pre-salt at the shallowest depth of the underlying reservoir at the absolute crest of the anticline (Fig. 3B). This common exit point of the fluids from the deep reservoir into the salt and beyond is consistent with the lateral transfer of overpressure, which predicts crestal bleed-off of overpressured cells (Flemings et al., 2002). Subsequent shearing by salt flow would have been incrementally smaller for each succeeding pockmark-pipe structure. This interpretation explains the lack of coherence in the reflection character of the interval overlying Reflection X, and the trail of amplitude anomalies seen on horizontal RMS amplitude slices through the salt (Fig. 2B; Fig. DR3).

The deformed pipe geometry demonstrates conclusively that the overburden was fully coupled to the salt throughout the Pliocene to Recent with no detachment. The rooting of 21 separate pipes to the crest of the anticline strongly implies that the flow within the salt approached a velocity of zero at its base, and hence that there was no localized detachment at the base of the salt. The flow direction is implicit from the orientation of the pockmark trail. This WNW orientation of flow is independently validated by orientations of fold axes in the nearby contractional domain immediately downdip of the trail and strike data for fault planes mapped in the updip extensional domain (Cartwright and Jackson, 2008)(Fig. 1B).

Publisher: GSA
Journal: GEOL: Geology
DOI:10.1130/G40219.1

The linear diachronous trail of pockmarks thus records two important parameters for salt tectonics that have not previously been quantified on a geological time scale. Firstly, by dating the oldest pockmark in the trail, and recording the flow distance over that time interval, the flow velocity of the upper boundary of this thick salt sheet can be calculated to be 2 (+/– 0.3) mm/a. Secondly, the geometry of the frontal deformed pipe records the cumulative strain in the flow direction, and this provides a direct constraint on the dominant mode of the flow regime operative during this interval of c. 1.7 Ma. The gently curved geometry of this deformed pipe closely approximates pure Couette Flow, although it should be noted that this geometry is subject to the usual limitations of seismic resolution, and any minor irregularities in the flow profile would probably be smoothed by the seismic imaging. Nevertheless, had there been a substantial component of flow driven by body forces (Poiseulle), a distinctively more parabolic geometry would be expected (Weijermars and Jackson, 2014). Couette flow is expected to occur where the salt deformation is dominantly driven by shear traction imposed from a translating overburden that is detached upslope, which in the case of the Levant Basin is achieved by the activity of an array of growth faults coupled to the general westward tilting of the basin (Cartwright and Jackson, 2008).

The average velocity measured for the top surface of the salt sheet allows us to compute the shear strain rate (4.10^{-14}) and the dynamic viscosity ($2.3.10^{18}$ Pa s) (see Data Repository) both of which are average values for the c. 1.7 Ma time period represented by the fluid escape pipes. These values are within the range of values for strain rate and dynamic viscosity derived from studies of salt diapirs and salt extrusions, and from laboratory-derived flow laws for common evaporite minerals (Urai and Spiers, 2007;

Urai et al., 2008). The viscosity value is based on the assumption of a Newtonian rheology, a homogeneous salt composition, a constant tilt of the top salt based on the present day value, and constant temperature within the salt, all of which grossly simplify the likely natural conditions (see Urai et al., 2008). Nevertheless, this does not diminish the potential value of identifying a strain marker within the salt sheet at the scale that allows its full vertical kinematic evolution to be constrained.

The highly overpressured conditions described here for the formation of these fluid escape pipes are by no means exceptional or unique in regions with thick salt deposits (Bertoni et al., 2017). Deformed fluid escape pipes should therefore be expected to occur elsewhere in the Messinian salt basin, and in other salt basins. The recognition of this new class of exceptionally large dimension strain markers represented by the deformed fluid escape pipes described here, thus offers the prospect of much improved constraints on the large-scale kinematics of deforming, basin-scale salt sheets and the testing of theoretical and experimental models for low strain rate salt deformation on a geological time scale.

CONCLUSIONS

1. Seismic data reveals a linear trail of 21 fluid escape pipes in the Levant Basin that formed episodically over the last 1.7 Myrs due to overpressuring beneath the 1.5 km thick Messinian evaporites.
2. The fluid escape pipes were deformed by WNW directed flow of the salt sheet after they formed, and hence represent a novel class of strain marker for evaluation of salt kinematics.

3. The oldest deformed pipe has a gently curvilinear geometry suggesting the cumulative flow of the salt sheet over this period closely approximated Couette Flow, with top and base salt coupled to overburden and substrate, respectively.
4. The average flow velocity was 2 mm/yr, which equates to a shear strain rate of 4.10^{-14} and a viscosity of $2.3.10^{18}$ Pa s.
5. This is the first in situ measurement of salt sheet viscosity on a geological time scale, and lies within the range of experimentally predicted values.

ACKNOWLEDGEMENTS

We are grateful to the editor and reviewers Chris Talbot, Janos Urai and Peter Kukla for their insightful comments that led to improvements in the manuscript. Schlumberger are acknowledged for provision of the seismic interpretation software. Chris MacMinn and Martino Foschi are thanked for many helpful discussions. This paper is dedicated to the memory of Martin Jackson, mentor and true friend.

REFERENCES CITED

Bertoni, C., and Cartwright, J.A., 2007, Major erosion at the end of the Messinian Salinity Crisis: Evidence from the Levant Basin, Eastern Mediterranean: Basin Research, v. 19, p. 1–18, https://doi.org/10.1111/j.1365-2117.2006.00309.x.

Bertoni, C., Kirkham, C., Cartwright, J., Hodgson, N., and Rodriguez, K., 2017, Seismic indicators of focused fluid flow and cross-evaporitic seepage in the Eastern Mediterranean: Marine and Petroleum Geology, v. 88, p. 472–488, https://doi.org/10.1016/j.marpetgeo.2017.08.022.

Brun, J.P., and Fort, X., 2011, Salt tectonics at passive margins: Geology versus models: Marine and Petroleum Geology, v. 28, p. 1123–1145, https://doi.org/10.1016/j.marpetgeo.2011.03.004.

Cartwright, J.A., and Jackson, M.P.A., 2008, Initiation of gravitational collapse of an evaporite basin margin: The Messinian saline giant, Levant Basin, eastern Mediterranean: Geological Society of America Bulletin, v. 120, p. 399–413, https://doi.org/10.1130/B26081X.1.

Cartwright, J., Jackson, M., Dooley, T., and Higgins, S., 2012, Strain partitioning in gravity-driven shortening of a thick, multilayered evaporite sequence, *in* Alsop, G.I. et al., eds., Salt Tectonics, Sediments and Prospectivity: Geological Society, London, Special Publication 363, p. 449–470, https://doi.org/10.1144/SP363.21.

Cartwright, J., and Santamarina, C., 2015, Seismic characteristics of fluid escape pipes in sedimentary basins: Implications for pipe genesis: Marine and Petroleum Geology, v. 65, p. 126–140, https://doi.org/10.1016/j.marpetgeo.2015.03.023.

Feng, Y.E., Yankelzon, A., Steinberg, J., and Reshef, M., 2016, Lithology and characteristics of the Messinian evaporite sequence of the deep Levant Basin, eastern Mediterranean: Marine Geology, v. 376, p. 118–131, https://doi.org/10.1016/j.margeo.2016.04.004.

Flemings, P.B., Stump, B.B., Finkbeiner, T., and Zoback, M., 2002, Flow focusing in overpressured sandstones: Theory, observations, and applications: American Journal of Science, v. 302, p. 827–855, https://doi.org/10.2475/ajs.302.10.827.

247 Gemmer, L., Ings, S.J., Medvedev, S., and Beaumont, C., 2004, Salt tectonics driven by
248 differential sediment loading: stability analysis and finite element experiments: Basin
249 Research, v. 16, p. 199–218, https://doi.org/10.1111/j.1365-2117.2004.00229.x.
250 Gradmann, S., Hübscher, C., Ben-Avraham, Z., Gajewski, D., and Netzeband, G., 2005,
251 Salt tectonics off northern Israel: Marine and Petroleum Geology, v. 22, p. 597–611,
252 https://doi.org/10.1016/j.marpetgeo.2005.02.001.
253 Gvirtzman, Z., Reshef, M., Buch-Leviatan, O., and Ben-Avraham, Z., 2013, Intense salt
254 deformation in the Levant Basin in the middle of the Messinian Salinity Crisis: Earth
255 and Planetary Science Letters, v. 379, p. 108–119,
256 https://doi.org/10.1016/j.epsl.2013.07.018.
257 Jackson, M.P.A., and Hudec, M.R., 2017, Salt Tectonics: Principles and Practice.
258 Cambridge, UK, Cambridge University Press, 510 p,
259 https://doi.org/10.1017/9781139003988.
260 Judd, A., and Hovland, M., 2009, Seabed fluid flow: the impact on geology, biology and
261 the marine environment: Cambridge, UK, Cambridge University Press, 492 p.
262 Kirkham, C., Cartwright, J., Hermanrud, C., and Jebsen, C., 2017, The genesis of mud
263 volcano conduits through thick evaporite sequences: Basin Research, v. 30, p. 217–
264 236, doi.org/10.1111/bre.12250.
265 Kukla, P.A., Reuning, L., Becker, S., Urai, J.L., Schoenherr, J., 2011, Distribution and
266 mechanisms of overpressure generation and deflation in the Late Neoproterozoic to
267 Early Cambrian South Oman Salt Basin. Geofluids, v. 11, p. 349-361, doi:
268 10.1111/j.1468-8123.2011.00340.x

Li, S., Abe, S., Urai, J., Strozyk, F., Kukla, P. and Van Gent, H., 2012, A method to evaluate long-term rheology of Zechstein salt in the Tertiary, *in* Berest, P., Goreychi, M., Hadj-Hassen, F., Tijani, M., eds., SaltMech7 - The mechanical behaviour of salt VII: London, Taylor and Francis, p. 215-220.

Reiche, S., Hübscher, C., and Beitz, M., 2014, Fault-controlled evaporite deformation in the Levant Basin, Eastern Mediterranean: Marine Geology, v. 354, p. 53–68, https://doi.org/10.1016/j.margeo.2014.05.002.

Urai, J.L. and Spiers, C.J., 2007, The Effect of Grain Boundary Water on Deformation Mechanisms and Rheology of Rocksalt During Long-Term Deformation, *in* Wallner, M., Lux, K., Minkley, W. and Jr., H.H. eds., Proceedings of the 6th Conference on the Mechanical Behaviour of Salt: Taylor and Francis, London, p. 149-158.

Urai, J.L., Schléder, Z., Spiers, C.J. and Kukla, P.A., 2008, Flow and Transport Properties of Salt Rocks, *in* Littke, R., Bayer, U., Gajewski, D. and Nelskamp, S., eds., Dynamics of Complex Intracontinental Basins: The Central European Basin System: Springer-Verlag, Berlin, Heidelberg, p. 277-290.

Weijermars, R., and Jackson, M.P., 2014, Predicting the depth of viscous stress peaks in moving salt sheets: Conceptual framework and implications for drilling: The American Association of Petroleum Geologists Bulletin, v. 98, p. 911–945, https://doi.org/10.1306/09121313044.

FIGURE CAPTIONS

Figure 1. Stratigraphy of the North Levant Basin and deformation pattern of the Messinian salt sheet. A: Location of the study area on a bathymetric map of the Eastern Mediterranean, with locations of exploration wells used for calibration. B: Map of the extensional domain and folds in the Plio-Pleistocene offshore Lebanon. C: Stratigraphic column of the Neogene in the study area. D: Cross-section through the extensional and contractional domains of the North Levant Basin. Sf – Seafloor; M – Top Salt; N – Base Salt; BMM – Base Mid Miocene; OU – Oligocene Unconformity.

Figure 2. Seismic characteristics of multi episode fluid escape from a single locus. A: Base Mid Miocene (BMM) contour map of NNE-SSW oriented fold and the location of 21 linearly distributed pockmarks (PM) that overly. B: Seismic profile through the linear trail of pipes (P). C: Seismic profile through a single pipe in the linear trail. D: Seismic profile oblique to the pipe trail through nearby amplitude anomalies (AA). TAA – Trail of amplitude anomalies; M – Top Salt; N – Base Salt; X – Reflection X; G/C B – Gelasian/Calabrian boundary.

Figure 3. Geological evolution of the trail of deformed fluid escape pipes. A: At 1.7 Ma, initial pipe (P) propagates from a folded Early Miocene reservoir and transects the overlying units, terminating in a pockmark (PM) at the seafloor (Sf). B: Subsequent pipes are located above crest of Fold A but are deformed during continuous salt flow (dotted lines). C: Present Day: linear trail of 21 pipes defines a progressive internal deformation of the salt sheet by Couette Flow. M – Top Salt; N – Base Salt; BMM – Base Mid Miocene; OU – Oligocene Unconformity; X – Reflection X.

Publisher: GSA
Journal: GEOL: Geology
DOI:10.1130/G40219.1

1GSA Data Repository item 2018xxx, xxxxxxxx, is available online at http://www.geosociety.org/datarepository/2018/ or on request from editing@geosociety.org.

Figure 1

Click here to download Figure Fig 1 Geology.jpg

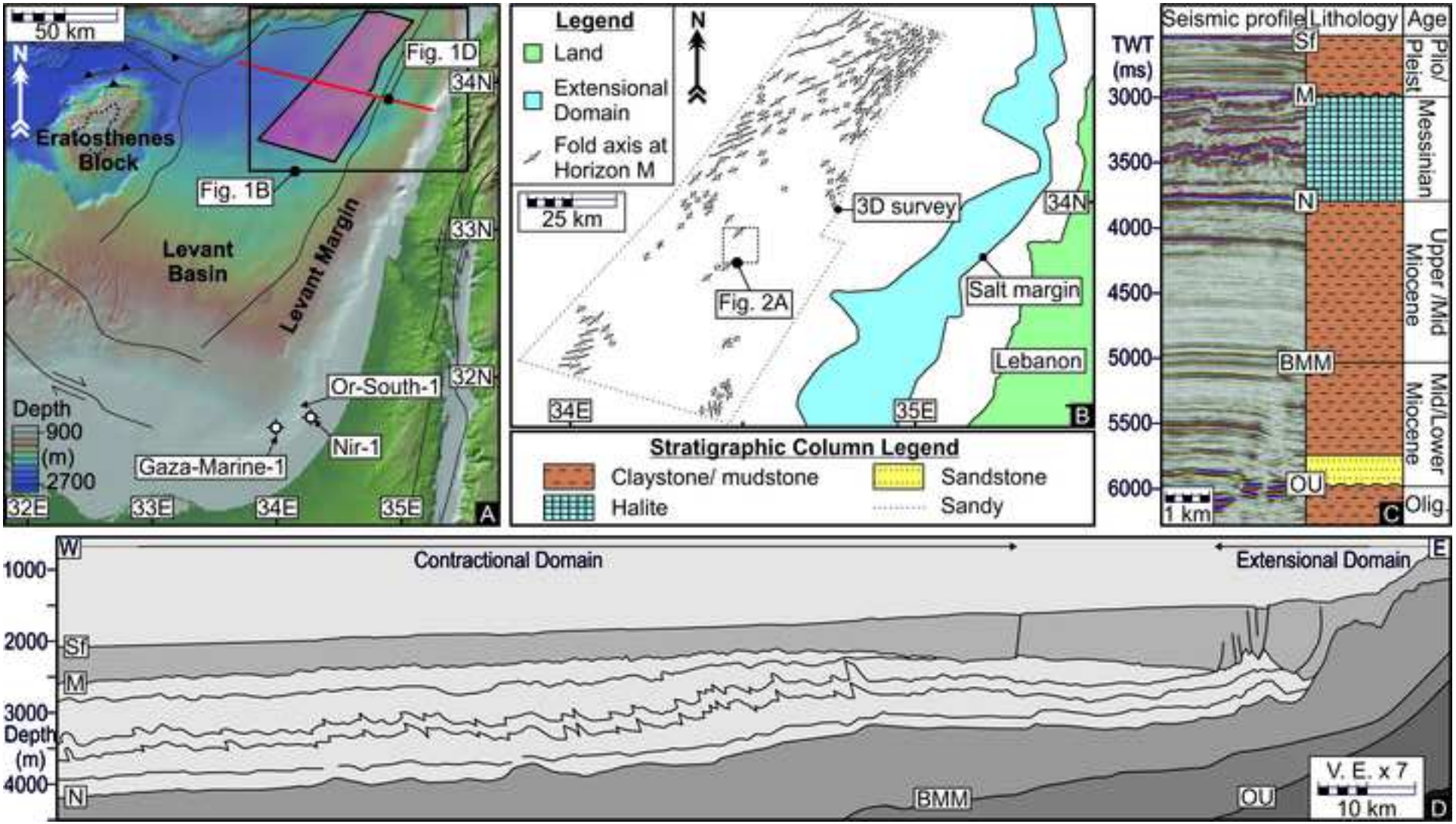

Figure 2

Click here to download Figure Fig 2 Geology.jpg

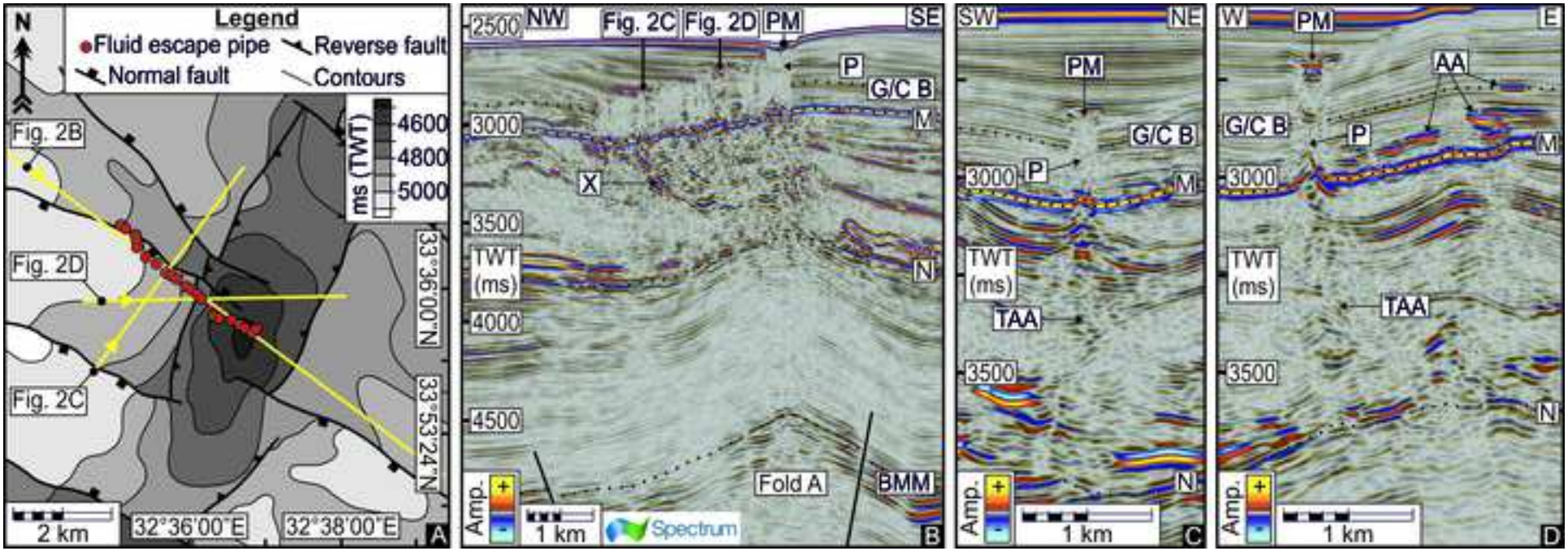

Figure 3

Click here to download Figure Fig 3 Geology.jpg

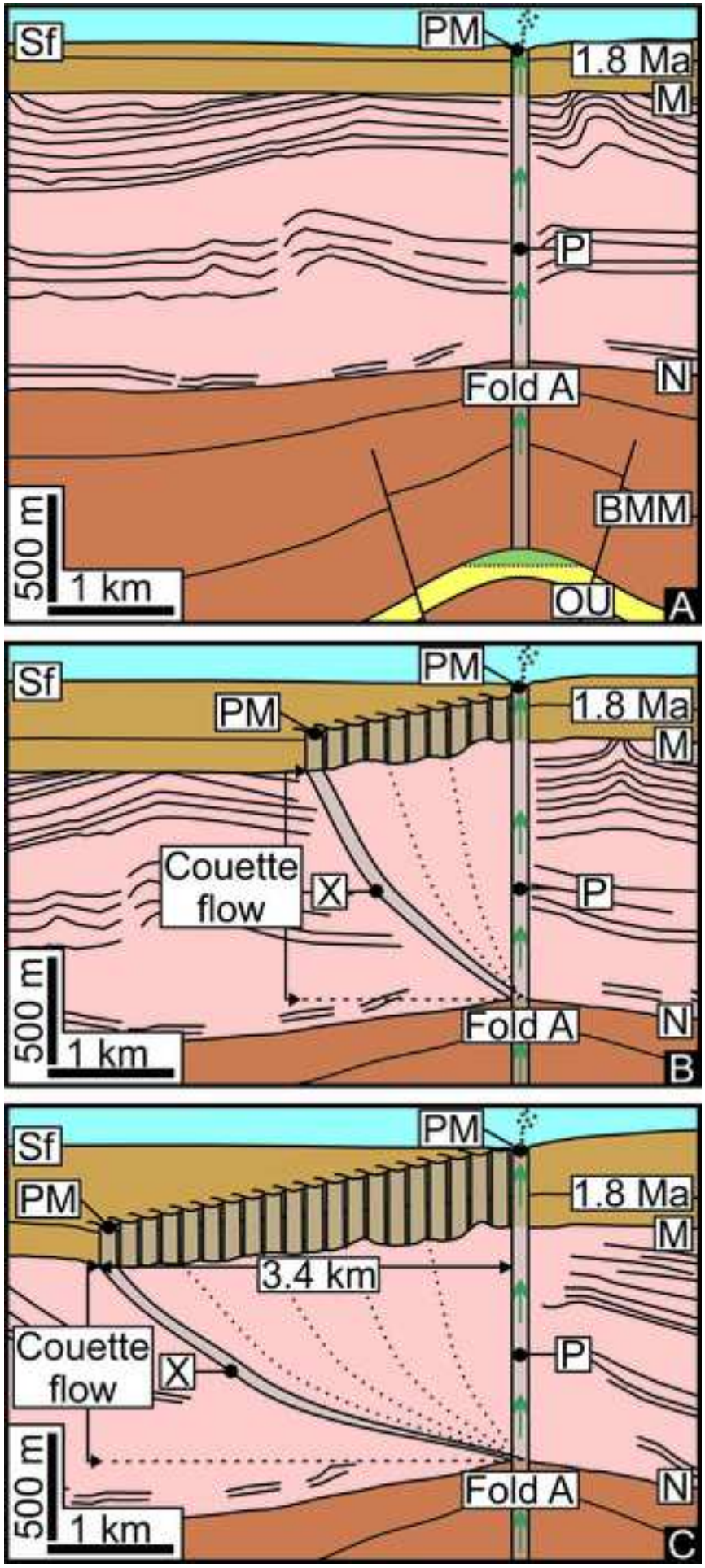

GSA DATA REPOSITORY

Supplementary material for "Direct calibration of salt sheet kinematics during gravity-driven deformation"

Joe Cartwright[1], Chris Kirkham[1], Claudia Bertoni[1], Neil Hodgson[2] and Karyna Rodriguez[2].

Seismic and well database

The data volume is post-stack time migrated, processed to a zero phase wavelet, and displayed with a polarity such that acoustically hard reflections (increase of acoustic impedance downwards) appear as positive amplitudes. The bin spacing is 12.5 m giving an effective lateral resolution of 25 m in the interval of interest. Dominant frequency is 50 and 30 Hz in the post-Messinian and Messinian intervals, respectively. The average P wave velocity for the post-Messinian interval is 2,000 m/s (based on nearby exploration wells Or-South-1, Nir-1 and Gaza-Marine-1; Fig. 1A; Fig. DR4) resulting in a vertical resolution of 10 m, based on the standard quarter wavelength criterion (Brown, 2011). The P wave velocity for the Messinian of 4,200 m/s is taken from exploration wells that drilled through the salt sheet to the southwest of the study area (Feng et al., 2016) giving a vertical resolution of 35 m within the salt. These velocities were used for depth conversion, along with an estimated 3,000 m/s for the pre-Messinian interval. Stratigraphic calibration of the key marker horizons in the 3D seismic survey were provided by long range correlations to exploration boreholes Or-South-1, Nir-1 and Gaza-Marine-1 (Fig. DR4).

Interpretation criteria for identification of pockmarks and fluid escape pipes

Pockmark craters were interpreted according to standard seismic interpretation criteria including a circular planform, crater-like morphology and incision at their base (Judd and Hovland, 2009). The absence of any seismically resolvable fill in the seafloor pockmark was used to infer a probable Holocene age (c.f. Reiche et al., 2014). Fluid escape pipes were interpreted based on diagnostic seismic features including loss of reflection coherency in a cylindrical zone, anomalous amplitude reflections within and immediately surrounding the pipe, and an upper termination in a pockmark crater (Moss and Cartwright, 2010; Cartwright and Santamarina, 2015)(Fig. 2; Figs. DR2 & DR3). Imaging challenges for interpreting fluid escape pipes within thick salt layers were taken into account (Kirkham et al., 2017) and contribute to positioning uncertainties for the calculation of flow velocity. This primarily affects the detailed measurement of pipe diameter, rather than the center points of pipes or pockmarks. Reflection X (Fig. 2) was interpreted by connecting the most frontal circular amplitude anomaly identified on closely spaced amplitude slices through the volume. Each circular anomaly was digitised for each slice, and an interpolation routine was used to connect the individual anomaly outlines into a volumetric body (Fig. DR1).

Dating key seismic horizons

Marker horizons were correlated to petroleum exploration wells further south in the basin using the 3D seismic data and a regional 2D seismic survey (Fig. DR4). The nearest boreholes that provide an age calibration for the important marker defining the

formation of the earliest pockmark are Nir-1, Or-South-1 and Gaza-Marine-1 offshore Gaza, some 240 km to the south (Fig. 1; Fig. DR4). The well ties indicate a Calabrian age for this onset marker horizon (c. 1.7 +/- 0.3 Ma), based on calibration of the Gelasian-Calabrian boundary. The boundary is dated at 1.806 My (Gradstein et al., 2012), and was identified in biostratigraphic well reports through the recognition of index taxa. The shallowest and last occurrence of *D. brouweri* is a regional marker for the top of Zone NN18 (1.95 Ma)(Catalano et al., 1998). The lowermost section of the Calabrian is defined by the downhole decrease in the recovery of *Gephyrocapsa spp*. (Rio et al., 1997) and the first occurrence of *G.tenellus*, *B. etnea* and *H. baltica* (Barbieri et al., 1998). These observations define the Gelasian-Calabrian boundary on seismic data within a range of error of approximately 150 ky (Fig. DR4). The uncertainty reflects the errors implicit in long range seismic correlation and in correctly picking the zonal fossils used to date the horizon. The top and base of the Messinian Evaporites are confidently identified by correlation to well ties in the area of the Tamar Field, some 60 km to the southwest (Feng et al., 2016)(Fig. 1a).

Salt Flow Kinematics

The average flow velocity for the upper boundary of the salt sheet was calculated from the biostratigraphic date for the horizon incised by the earliest pockmark, and the horizontal distance between the earliest and latest pockmark craters (3.4 km)(Fig. DR1). These values give an average flow velocity of 2 (+/- 0.3) mm/a over the past 1.7 myrs. The shear strain rate of $4.23.10^{-14}$ was calculated from the average velocity divided by the salt sheet thickness (1500 m), making the important assumption that the sheet did not thin during this time interval. The dynamic viscosity was calculated

by dividing the shear stress by the shear strain rate (Barnes et al., 1989), assuming a Newtonian rheology and homogenous composition for the salt sheet. Both of these assumptions are questionable, although at low temperature, and slow strain rate the salt deformation could be expected to be dominated by solution-precipitation creep which would be consistent with a Newtonian rheology (Jackson and Hudec, 2017). Thin interbeds of claystones have been inferred within the salt from analysis of petrophysical logs acquired in exploration boreholes further south in the basin (Feng et al. 2016), and these would certainly influence the gross behaviour of the salt. We also assumed a constant temperature profile through the salt, which is a gross simplification, but have no data on temperature variations within, above or below the salt.

The salt was assumed to deform dominantly by shear traction at the upper boundary of the salt sheet, consistent with the idealised boundary conditions for Couette Flow (Weijermaars and Jackson, 2014). Shear stress was calculated for a present day overburden tilt of 0.7˚ measured from a depth converted seismic profile (Fig. 1D) using a standard analytical approach for Couette Flow (Weijermaars and Jackson, 2014) and assuming an overburden thickness of 400 m (present day), and a density averaging 2000 kg/m^3. Earlier pipes may have formed with tilt angles different from that today, and we assumed a range of 0.1 to 2˚ based on analysis of the reflection configurations and isopach patterns in the Late Pliocene to Pleistocene interval. These values yielded viscosity values ranging from $3.22.10^{17}$ to $6.6.10^{18}$ Pa.s (present day value is $2.27.10^{18}$ Pa.s) which is within the range quoted from theoretical and field studies of evaporites dominantly composed of halite (Jackson and Hudec, 2017).

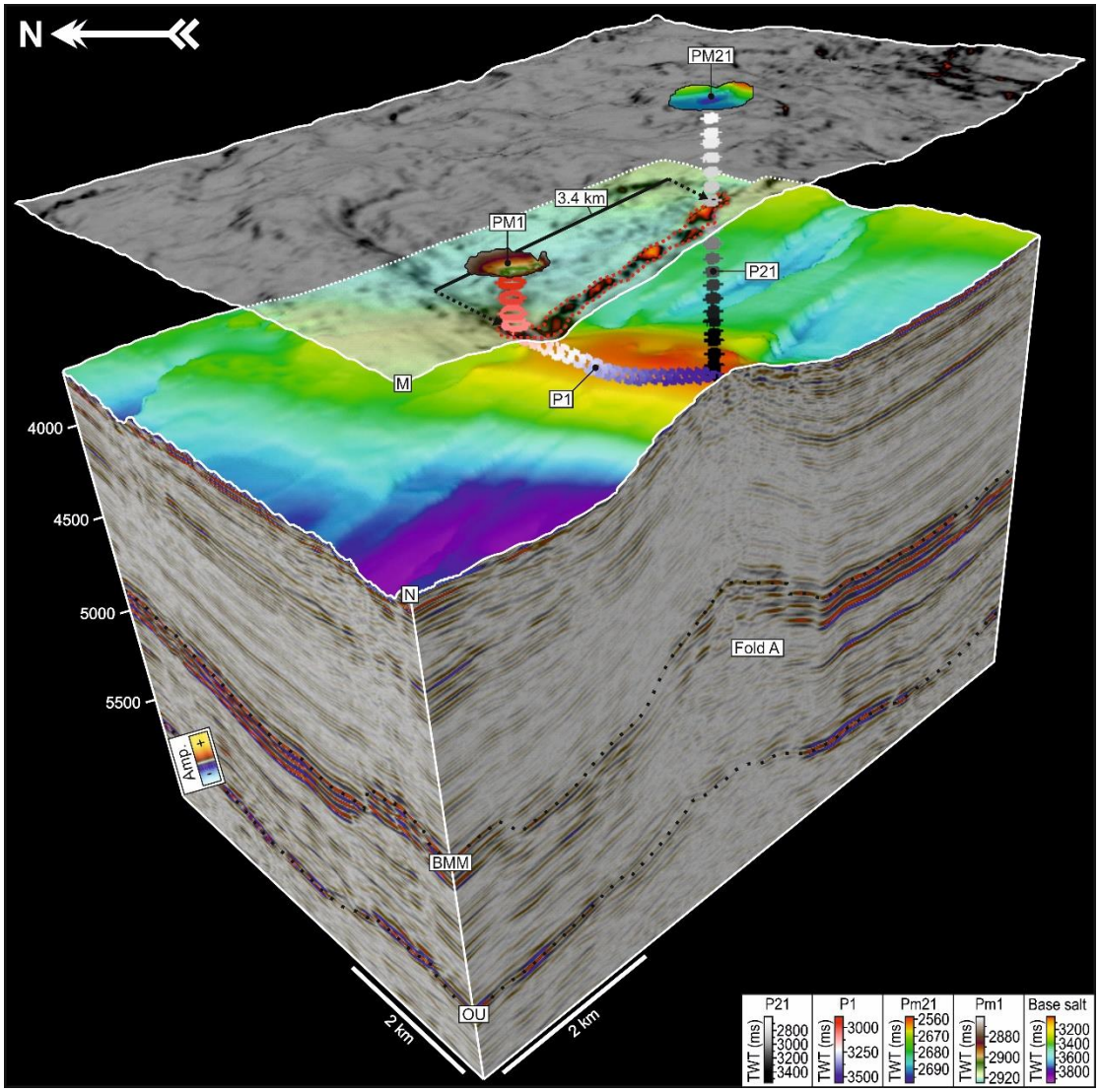

Figure DR1: A three dimensional block model of the first and most recent fluid escape pipes (P1 and P21), emanating from the crest of the anticline Fold A. The pipes terminate at pockmarks located at individually specific stratigraphic levels, successively younging towards the ESE. The distance between the first and most recent pockmarks is 3.4 km. The trail of pipes produces a WNW-ESE oriented trail of reflection discontinuity as exhibited in the variance extraction map of the top surface of the evaporites (M) and highlighted by the red dotted outline. Three dimensional mapping of the pipes through the salt displays a columnar structure for the most recent pipe (P21) and a gently curvilinear geometry to the first pipe (P1) that closely approximates that which would be expected from Couette Flow through the salt. OU –

Oligocene Unconformity; BMM – Base Mid Miocene; N – Base salt; PM1 – Pockmark 1; PM21 – Pockmark 21.

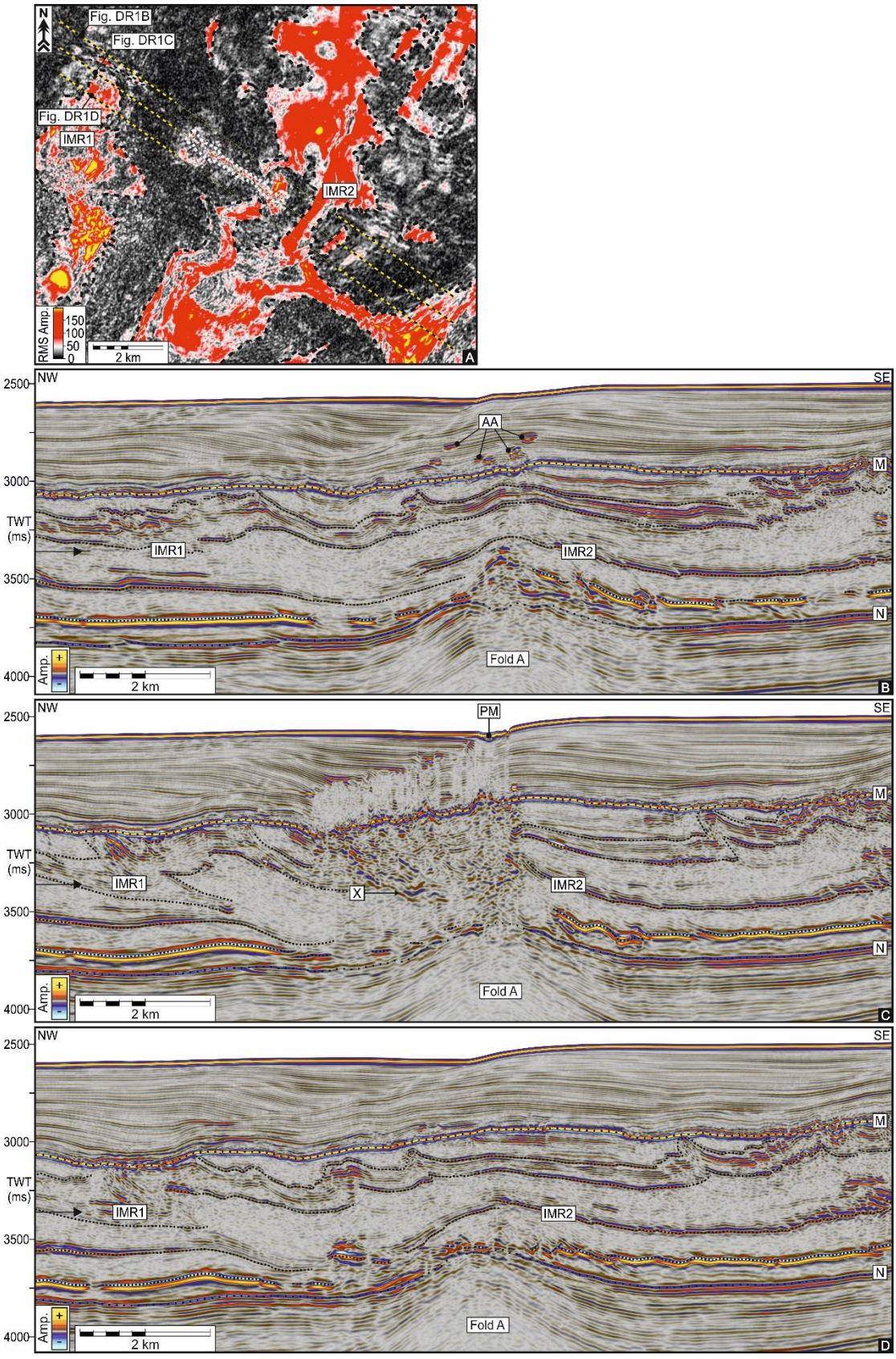

Figure DR2: Seismic profiles 500 m either side of the pockmark trail and Reflection X, demonstrating that the geometry of intra-salt reflections is similar on both sides

and contrasts with the geometry of Reflection X. Reflection X was hence superimposed over an already deformed evaporitic succession.

(A) An RMS amplitude slice (3363 ms (see black arrow on seismic profiles); Fig. DR2B-D for position of slice) through the pipe trail in the salt (highlighted by white dotted line) and numerous intra-Messinian stratal anomalies (highlighted by black dashed line). The lines of section for Fig. DR2B-D are displayed and the deformed intra-Messinian reflections (IMR1 and IMR2) that these seismic profiles intersect are highlighted. (B) A seismic profile 500 m to the northeast of the pipe trail exhibiting numerous reflective layers within the evaporitic succession. Fold A is present within the seismic profile; however no fluid escape pipes are visible within the evaporitic or Plio-Pleistocene sequences. The intra-Messinian reflections highlighted in Fig. DR2A (IMR1 and IMR2) are also highlighted here. Several amplitude anomalies (AA) that are acoustically soft are displayed within the Plio-Pleistocene. (C) A seismic profile through the pipe trail that shows an area of vertical discontinuities within the Plio-Pleistocene which is underlain by an acoustic fabric and the coherent reflection of Reflection X, which is discordant to the intra-Messinian reflections. The intra-Messinian reflections highlighted in Fig. DR2A are also highlighted here (IMR1 and IMR2). (D) A seismic profile 500 m to the southwest of the pipe trail that exhibits numerous intra-Messinian reflections (also highlighted in Fig. DR2A) that display similar geometries to the cross-section in Fig. DR2B and shows no evidence of the fluid escape pipes, acoustic fabric or Reflection X seen in Fig. DR2C. M – Top salt; N – Base salt.

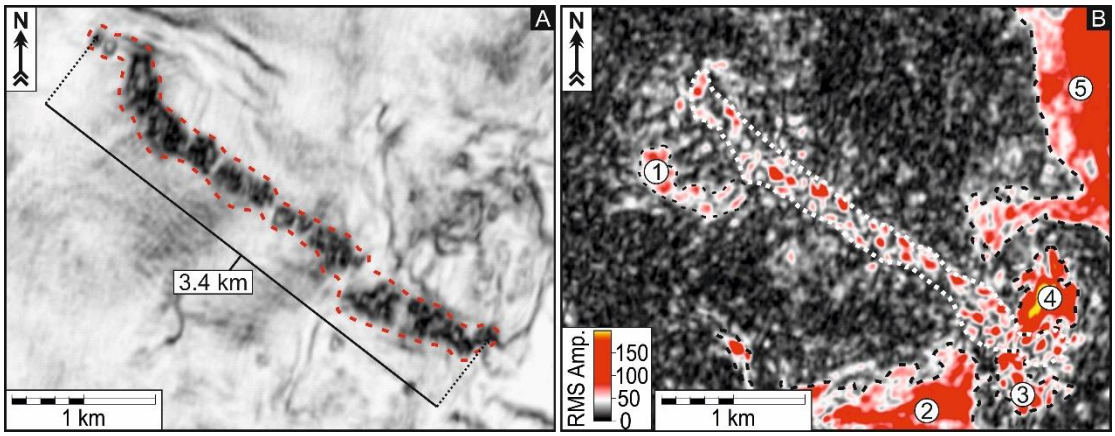

Figure DR3: (A) A WNW-ESE oriented distribution of fluid escape pipes in the Pliocene to Recent, expressed in a horizontal slice of the coherence attribute volume (2912 ms) as a linear trail of circular to sub-circular discontinuities (highlighted by red dashed line). (B) An RMS amplitude horizontal slice (3364 ms) through the evaporitic unit at the exact same spatial location as in Fig. DR3A. The fluid escape pipes appear as a localised WNW-ESE oriented trail of amplification (highlighted by white dotted line). Intra-salt stratal anomalies (labelled 1-5 and highlighted by black dashed lines) exhibit contrasting geometrically irregular areas of high amplitude.

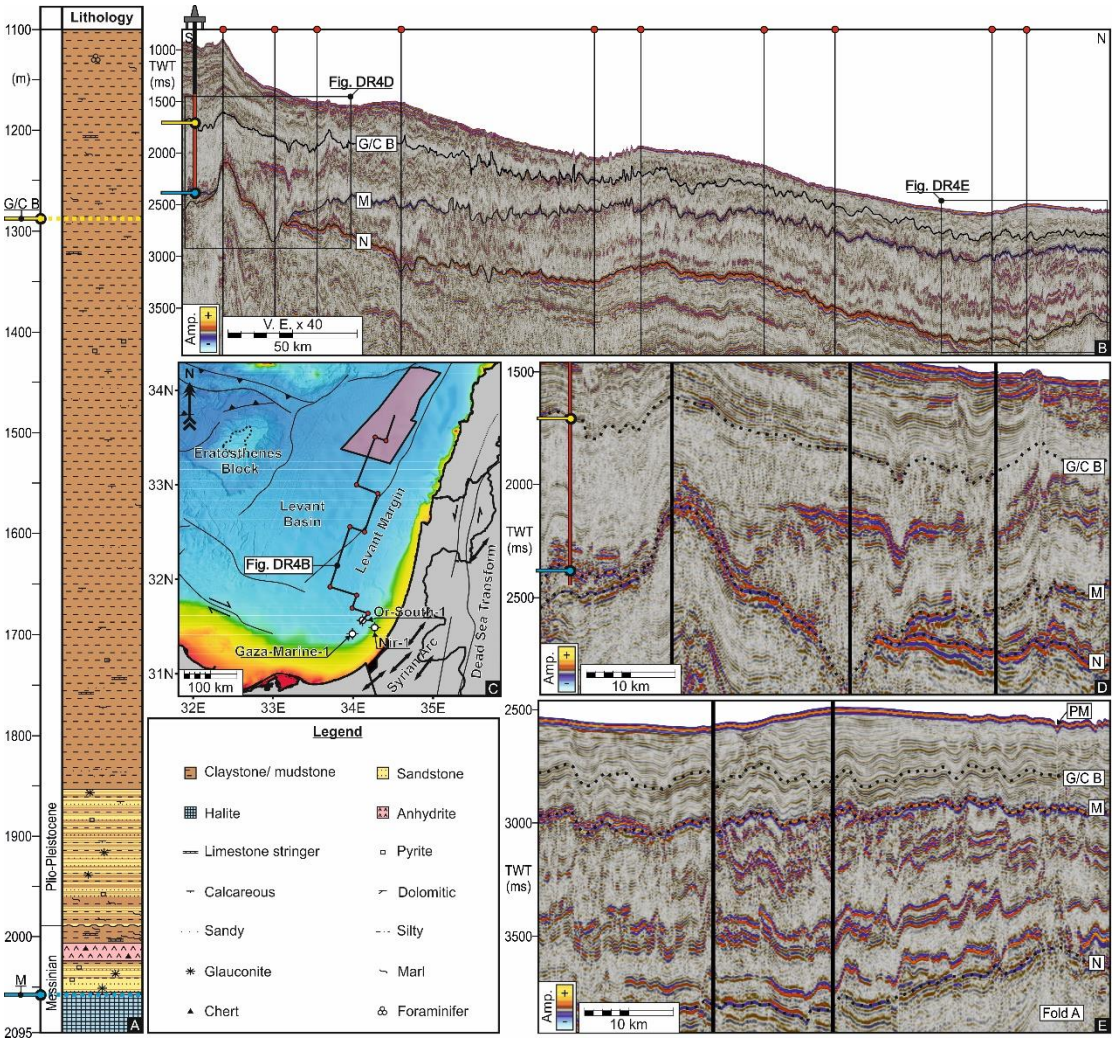

Figure DR4: Seismic to well tie. The well data aided the calibration of the top of the salt (M) and of the Gelasian/Calabrian boundary 1.806 Ma (G/C B). (A) A section of the stratigraphic column from the Or-South-1 well that extends from a depth of 1100 m within the Pleistocene to a total depth of 2095 m where it terminates in the evaporites. The well shows detailed lithological variation and the boundaries between the top of the salt (M) and the Plio-Pleistocene sequences, and the boundary between the Gelasian and Calabrian. (B) A composite seismic cross-section (see Fig. DR4C for location) that extends from the South Levant Basin to the 3D seismic survey area in the North Levant Basin and shows the long range calibration of key marker horizons from the Or-South-1 well. (C) Map of the Levant Basin that displays the location of the 3D seismic study area offshore Lebanon, and the location of the Gaza-Marine 1,

Nir-1 and Or-South-1 wells in the South Levant Basin used for the well to seismic tie. The position of the composite line used in Fig. DR4B to demonstrate the long range calibration of key marker horizons is shown. (D) A zoomed-in (close up) seismic profile from the South Levant Basin (see Fig. DR4B for location) showing our interpretation of key marker horizons. (E) A zoomed-in seismic profile from the North Levant Basin (see Fig. DR4B for location) showing our interpretation of key marker horizons.

REFERENCES

Brown, A.R., 2011, Interpretation of three-dimensional seismic data: Society of Exploration Geophysicists and American Association of Petroleum Geologists, 665 p.

Barbieri, M, Castorina, F., Colalongo, M.L., Pasini, G., and Vaiani, S.C., 1998, Worldwide correlation of the Pliocene/Pleistocene GSSP at Vrica (Southern Italy) confirmed by strontium isotope stratigraphy: Newsletters on Stratigraphy, v. 36, p. 177–187.

Barnes, H.A., Hutton, J.F. and Walters, K., 1989, An introduction to rheology (Vol. 3): Amsterdam, Elsevier, 200 p.

Catalano, R., Di Stefano, E., Sulli, A., Vitale, F. P., Infuso, S. & Vail, P. R., 1998, Sequences and Systems Tracts Calibrated by High Resolution Bio-

Chronostratigraphy: The Central Mediterranean Plio-Pleistocene Record: SEPM (Society of Sedimentary Geology) Special Publication, v. 60, p. 115-177,

Cartwright, J. and Santamarina, C., 2015, Seismic characteristics of fluid escape pipes in sedimentary basins: implications for pipe genesis: Marine and Petroleum Geology, v. 65, p. 126-140.

Feng, Y.E., Yankelzon, A., Steinberg, J. and Reshef, M., 2016, Lithology and characteristics of the Messinian evaporite sequence of the deep Levant Basin, eastern Mediterranean: Marine Geology, v. 376, p. 118-131.

Gradstein, F. M., Ogg, J. G., Schmitz, M., Ogg, G., 2012, The geologic time scale: Elsevier, 1176 p.

Jackson, M.P.A, and Hudec, M.R., 2017, Salt Tectonics: Principles and Practice: Cambridge, Cambridge University Press, 510 p.

Judd, A. and Hovland, M., 2009, Seabed fluid flow: the impact on geology, biology and the marine environment: Cambridge University Press, 492 p.

Kirkham, C., Cartwright, J., Hermanrud, C. and Jebsen, C., 2017, The genesis of mud volcano conduits through thick evaporite sequences: Basin Research, doi: 10.1111/bre.12250.

Moss, J.L. and Cartwright, J., 2010, 3D seismic expression of km-scale fluid escape pipes from offshore Namibia: Basin Research, v. 22, p. 481-501.

Reiche, S., Hübscher, C. and Beitz, M., 2014, Fault-controlled evaporite deformation in the Levant Basin, Eastern Mediterranean: Marine Geology, v. 354, p. 53-68.

Rio, D., Raffi, I., Backman, J., 1997, Calcareous nannofossil biochronology and the Pliocene-Pleistocene boundary, *in* Van Couvering J.A., ed., The Pleistocene Boundary and the Beginning of the Quaternary, World and Regional Geology 9: Cambridge University Press, p. 64-79.

Weijermars, R. and Jackson, M.P., 2014, Predicting the depth of viscous stress peaks in moving salt sheets: Conceptual framework and implications for drilling: American Association of Petroleum Geologists Bulletin, v. 98, p. 911-945.